https://doi.org/10.7494/geom.2025.19.6.5

Soni Darmawan¹, Rika Hernawati², Shafa Rahmani³

Satellite-Based Urban Heat Island Study: A Prisma-Based Systematic Literature Review

Abstract:

Over the years, urban heat island (UHI) has emerged as a significant contributor to global warming, thereby necessitating considerable attention. Currently, satellite technology is a basic tool for the future – particularly, for its effective and efficient urban analysis. Thus, this study aims to assess the progress of existing satellite-based UHI studies by reviewing scientific publications that were released between 1972 and early 2024. Moreover, we observed that 1991 was a pivotal year, marking the integration of satellite technologies into the development of UHI monitoring and identification systems based on the Preferred Reporting Items for Systematic Reviews and Meta-Analyses (PRISMA) guidelines, this review methodology examines the UHI phenomenon by focusing on its characteristics based on sensors, algorithms, and accuracy. The results of the systematic review revealed that Landsat and MODIS were the most-deployed sensors for UHI identification and monitoring, while the land surface temperature (LST) indicator and normalized difference vegetation index (NDVI) were the most-deployed algorithms. Regarding accuracy, the integration of satellite sensors and algorithms into UHI studies provides a promising range of accuracies. The review found that the future of satellite-based UHI monitoring is promising, with technological advancements driving the development of effective techniques such as data fusion, gap filling, machine learning (ML), and deep learning. Additionally, Google Earth Engine (GEE) is a cloud-based platform for performing large-scale geospatial analyses, which facilitates the assessments of local, regional, and global-scale UHIs. Finally, the other review findings for future directions indicated that future satellite-based UHI studies will prioritize six crucial points: enhancing data resolution, integrating satellite data with ground-based sensors, artificial intelligence, and ML, climate change modeling, and a global study of UHIs and their impacts.

Keywords: urban heat island, remote sensing, accuracy, machine learning, Google Earth Engine

Received: August 30, 2024; accepted: July 21, 2025

© 2025 Author(s). This is an open-access publication that can be used, distributed, and reproduced in any medium according to the Creative Commons CC-BY 4.0 License

Institut Teknologi Nasional Bandung, Bandung, West Java, Indonesia, email: soni_darmawan@itenas.ac.id (corresponding author), https://orcid.org/0000-0001-8637-0835

Institut Teknologi Nasional Bandung, Bandung, West Java, Indonesia, email: rikah@itenas.ac.id, https://orcid.org/0000-0002-0069-1572

³ Institut Teknologi Nasional Bandung, Bandung, West Java, Indonesia, email: shafaarhmn@gmail.com

1. Introduction

Urban heat island (UHI) is a phenomenon that describes the elevated temperatures that can be observed in metropolitan or urban areas owing to human activities (including the development and utilization of environmentally unfriendly motorized vehicles) [1]. This phenomenon indicates that the canopy layers of central urban regions exhibit higher excess temperatures than nearby regions at similar elevations [2]. UHIs contribute to natural-ecosystem degradation, deforestation, and biodiversity reduction [3]. Notably, the rapid development of cities has led to increased human activities, which frequently occur with little regard for their impacts on existing infrastructure and other essential urban functions [4]. UHIs are influenced by various factors, including geographical (climate, topography, and surrounding rural areas) and temporal (daily and seasonal) variations, meteorological conditions, city populations (the relationships between buildings and functions), synoptic weather conditions (wind and cloud covers), city form (materials, geometries, and green open spaces), and city functions (energy/water consumption and pollution) [2].

The existing UHI studies have employed surface-temperature models to establish the relationship between roadway geometries and nocturnal heat islands [5]. One method for enhancing human thermal comfort in urban spaces involves the exploration of strategies for mitigating the UHI phenomena (Fig. 1).

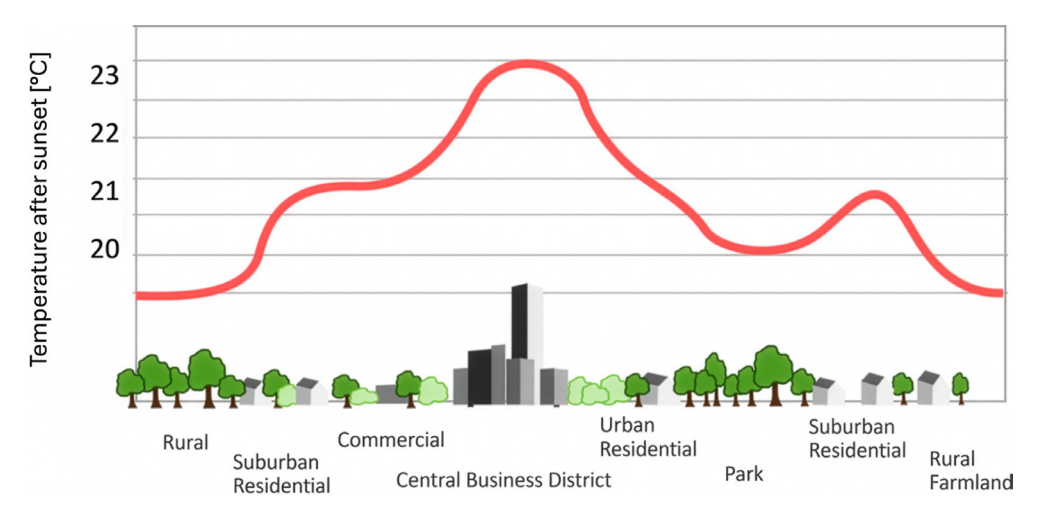


Fig. 1. UHI temperature profile Source: [6]

The consistent shape of a UHI temperature profile (Fig. 1) often corresponds to a depression that is formed by the existence of specific hotspots (micro-UHIs). The origins of these micro-UHIs are tied to factors such as parking lots, shopping centers,

and industrial facilities – some of them expanding because of specific heat [6]. The author of [5] further connected their origins to landscape elements that included fields, gardens, and water bodies. Moreover, a UHI's intensity or magnitude was defined as the difference between a city's peak temperature and the lowest temperature of its surrounding areas [7].

In 2005, the Environmental Protection Agency identified the UHI phenomenon as a major issue for cities globally [8]. The 2007 report of the Intergovernmental Panel on Climate Change confirmed that urbanization and land use (LU) changes only exerted negligible effects (less than 0.006°C and 0°C per decade over land and ocean, respectively) on the global temperature records [9]. Additionally, urbanization and LU exert negligible effects on the reported widespread warming of water bodies. However, evidence abounds regarding the impacts of UHIs on clouds, precipitation, and daily temperature ranges [10]. Over the years, UHIs have emerged as significant contributing variables to the occurrence of global warming [11]. Alongside natural catastrophes, precipitation, and increased sea levels, urban warming is a key driver of global change in cities, accounting for 60% of its causes [12]. UHIs impact the environment as well as human life, increasing air pollution and the accumulation of greenhouse gases (GHGs); this impacts urban living and poses health threats [13]. Increasing temperatures typically exacerbate human stress, thereby reducing urban people's productivity and creativity [13].

UHIs can develop at several urban-atmosphere levels, including surface and subsurface levels [2, 14]; this is a phenomenon where urban areas are warmer than their surrounding non-urban areas. Atmospheric heat islands dominate during calm and clear nights; these are characterized by a significant difference in radiative cooling between metropolitan and surrounding rural areas [14]. Basically, UHIs are known as surface UHIs and temperature UHIs; surface urban heat islands and temperature urban heat islands refer both to the phenomena in which urban areas show higher temperatures than their surrounding rural areas [15]. Surface UHIs particularly indicate the difference in land surface temperatures, whereas UHIs include both surface and air temperature differences [15, 16]. The advent of satellite remote-sensing technology has enabled surface UHI studies across larger areas [17].

Satellite remote-sensing techniques are basic research tools for the future – particularly for effective and efficient urban analysis (including UHI estimations) [17]. The advantages of using satellite remote-sensing data include their relatively high resolution, consistency, reproducibility, and capacity to accurately measure/record ground conditions [18]. In satellite remote sensing, satellites that are equipped with thermal-infrared (IR) and TIR sensors (TIRS) collect quantitative surface-temperature data for measurement and analysis [19]. In the last three decades, satellite-based UHI studies have solely focused on estimating surface temperatures from IR data. At first, most of these studies relied on the Advanced Very High-Resolution Radiometer (AVHRR) satellites of the National Oceanic and Atmospheric Administration [20]. The 1990s were characterized by the widespread utilization of IR bands

from Landsat Thematic Mapper (TM) satellites for urban climate studies, followed by the adoption of Enhanced TM Plus (ETM+) technology in the early 2000s for UHI estimation [21]. Several authors (including [21]) have reviewed UHI studies; e.g., Review on urban heat islands in China: methods, its impacts on building energy requirements and mitigation strategies. A literature review of the UHI model of a Malaysian tropical city [22] and another review that was conducted by [23] critically evaluated the existing UHI studies by highlighting their methodological shortcomings. However, only a few literature reviews have adopted the Preferred Reporting Items for Systematic Reviews and Meta-Analyses (PRISMA) technique – particularly for engineering reviews [24].

Several technical literature reviews followed the PRISMA approach; e.g., [25], which examined oil palm phenology modeling based on remote-sensing data. The review offered insights into the developments of appropriate identification, classification, and construction techniques for oil palm phenology regression models. Additionally, [26] investigated Buhos – a web-based systematic literature review (SLR) management application that was developed in Ruby and provided tools for search filtration, data extraction, and reporting. Buhos can be locally installed using an internal web server or disseminated and incorporated into other online services.

Thus, this SLR (Satellite-Based Urban Heat Island Study: A PRISMA-Based SLR) was conducted in response to the criticality of assessing the evolution of satellite-based UHI studies to explore references for future studies. This SLR is aimed at determining the progress of existing satellite-sensor-based UHI studies by reviewing scientific publications that were released between 1972 and early 2024. This review mainly focused on journals that were related to satellite-based UHI studies.

This paper is organized as follows. Section 2 contains the literature review of the main methods used in satellite-based urban heat island (UHI) studies. Section 3 presents the identification of UHI characteristics according to sensor type, algorithms, and accuracy. Section 4 discusses the results, while Section 5 outlines future directions for satellite-based urban heat island studies. Finally, Section 6 concludes the study.

2. Literature Review of Methods for Satellite-Based Urban Heat Islands

Employing the PRISMA approach, suitable journals were collected (starting from the earliest scientific publications) [24]. This approach followed a set of scientific techniques that was specifically designed to prevent bias – primarily by aiming to identify, appraise, and synthesize all of the relevant literature to answer the research questions [27].

The literature search was conducted from many databases; however, this review used Google Scholar and Scopus, as both database search engines were versatile on

the subject matter and were conventionally employed for literature searches [25]. The literature search was conducted using the following keywords: TITLE-ABS-KEY ("urban heat island" AND "remote sensing" AND "surface temperature" AND "vegetation index").

Consequently, our literature search generated 4400 journals that were published between 1972 and early 2024. Thereafter, we screened for any duplications that were included in the searches that were conducted on Google Scholar and Scopus (Fig. 2). In 1991, satellite remote-sensing–based studies for UHI monitoring and identification started to appear; e.g., studies that involved the utilizations of the IR bands from the Landsat TM satellites. Thus, we filtered the 4,400 papers, yielding 421 relevant papers. Additionally, we identified 56 journals that were re-filtered during the eligibility assessment, as they did not satisfy the inclusion requirements. This action yielded 29 journals for the SLR; these papers explored the most-recent satellite remote-sensing technologies that were relevant to this review.

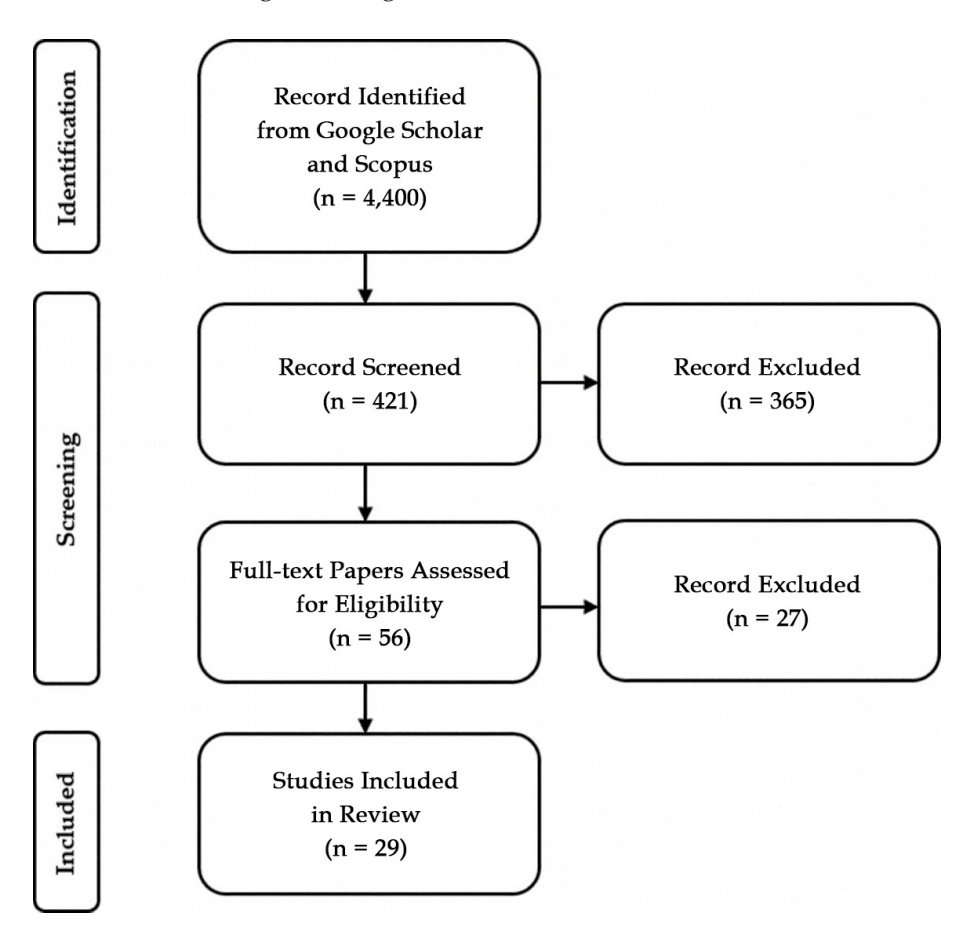


Fig. 2. PRISMA flowchart

Based on the development of satellite remote-sensing technology for UHI identification and monitoring that started in 1991 (Fig. 3), our review findings identified 421 relevant studies. The graph (Fig. 4) shows that only a few studies on UHI were published between 1991 and 2006; however, 2009 witnessed a significant increase in the number of UHI studies.

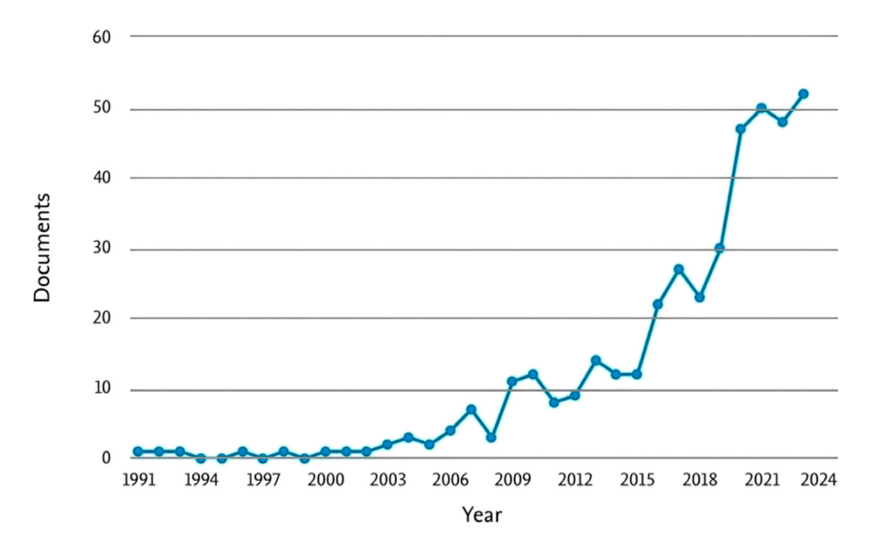


Fig. 3. Number of satellite remote-sensing-based UHI articles by publication year

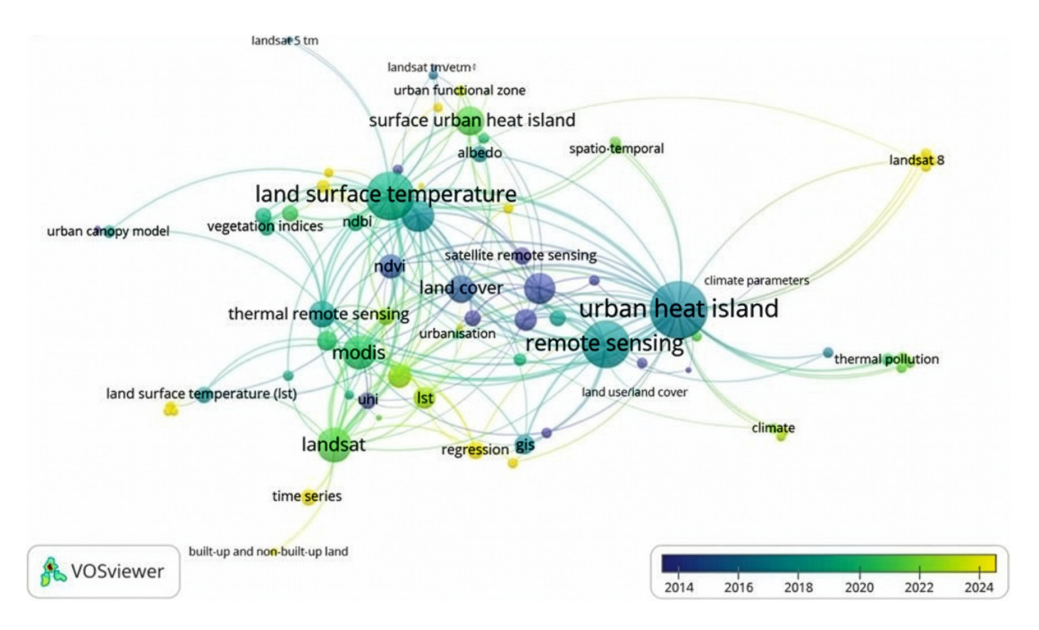


Fig. 4. Bibliometric analysis of review articles on UHI studies based on keywords and publication times

An increase in UHI studies could be observed again in 2018; this continued until early 2024. Notably, Scopus identified 23, 30, 47, and 50 publications in 2018, 2019, 2020, and 2021, respectively. Additionally, 48 and 52 publications were identified in 2022 and early 2024, respectively.

Our literature review of UHIs was categorized by keywords and a publication period using a bibliometric approach. Figure 4 shows the bibliometric analysis of the review articles on UHI studies by keyword and time (as was obtained from the filtered scientific publications). This visualization was implemented using VOSviewer software, which identified the relationship and keyword co-occurrences in the literature [25]. The visualization colors reflect the distribution of the average keyword-occurrence times, which was generated through an internal normalization process by VOSviewer. Put differently, the year ranges that are shown in the figure do not represent a fixed chronological time division; rather, they are arranged based on the frequency and temporal distribution of the keyword occurrences across the entire amount of data. In this figure, the dark-blue to light-blue colors reflect keywords that appeared earlier (2014–2018), and the green to light-yellow colors indicate those that appeared more recently and are relevant to recent studies (around 2019 through early 2024). Dominant keywords such as urban heat island, satellite remote sensing, land surface temperature, MODIS, and NDVI formed the main nodes with high association levels, thus reflecting the main focus of the UHI literature over the past decade. Furthermore, the latest trends are shown in yellow; they include keywords such as Landsat 8, time series, heat waves, and regression; these indicate the increasing attention to high-resolution data and time-series analysis in the UHI studies.

Figure 5 shows that the Scopus-detected journal publications on satellite remote-sensing-based UHIs were mostly published by seven web-based publishers. The International Journal of Remote Sensing published web-based journals on UHIs between 1992 and 1998. The web-based publication of The International Archive of the Photogrammetry, Remote Sensing and Spatial Information Sciences (International Society for Photogrammetry and Remote Sensing [ISPRS] Archives) started in 2000. The ISPRS Journal of Photogrammetry and Remote Sensing first published a journal on UHIs in 2003. The Proceedings of SPIE (The International Society for Optics and Photonics) published 29 journals from 2005 through early 2024. In 2012, Remote Sensing began publishing on UHIs through 2023, accounting for 21 web-published journals. However, The International Archives of the Photogrammetry, Remote Sensing and Spatial Information Sciences (ISPRS Archives) accounted for most of the journals on satellite-based UHIs that were detected by Scopus between 1991 and early 2024. Although the places that the web publication of Remote Sensing of Environment was not detected by Scopus between 2019 and early 2024, web-based journal publications by Proceedings of SPIE were detected between 2005 and 2021. Furthermore, Remote Sensing (Multidisciplinary Digital Publishing Institute, MDPI) was among the most frequently chosen journals for publishing UHI studies between 2012 and 2024.

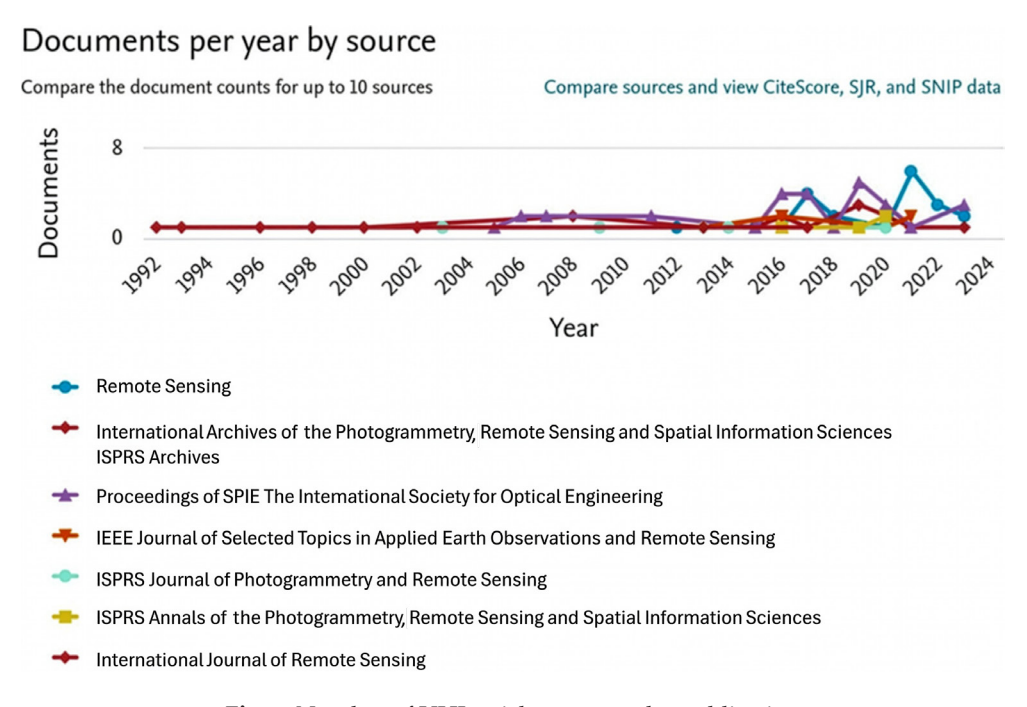


Fig. 5. Number of UHI articles per year by publication

3. Identification of Urban Heat Island Characteristics Based on Sensors, Algorithms, and Accuracy

The reviewed studies generally developed a novel approach for identifying and mapping the spatial distributions of UHIs based on sensor types, algorithm types, and accuracy.

3.1. Sensors

As has been demonstrated by several studies, satellite remote sensing offers significant benefits in UHI estimations owing to its ability to provide surface-radiance and surface-emissivity data [28]. The electromagnetic spectrum range (with wavelengths of 3–35 μ m) is known as the TIR band [29]. Furthermore, the radiation intensity and presence of atmospheric windows are key drivers of the selections of relevant spectral bands within this range [28]. A very effective atmospheric range for remote sensing exists between 8 μ m and 14 μ m (where most remote sensors are configured to measure the thermal radiative characteristics of ground materials) [14, 28]. The existing TIR satellite sensors recently provided spatial resolution and temporal coverage data that can be utilized to estimate the land-surface temperature (LST) – a significant parameter for measuring the radiative temperature of

the Earth's surface [2]. The thermal remote sensing of urban surface temperatures is a typical method for monitoring LSTs to modify a surface-energy balance [2]. The generated radiation is measured as a digital number (DN); after this, it is transformed into temperature data [5]. Satellite TIRS measures the top of the atmosphere (TOA) radiance that is emitted by the Earth's surface and atmosphere, including surface-emissivity-determined TOA radiances (built-up areas, vegetation, bare soil, etc.), the atmospheric attenuation (water vapor and aerosols), the angle at which a satellite sensor receives the radiation, the atmospheric window at 10– $12~\mu m$, and the relatively low absorption of the land-surface-emitted IR radiation [5]. Therefore, this spectral region is used to derive the LST using one or more IR bands [2].

Table 1. TIRS satellite source

Satellite Acquired	Wavelength [μm]	Spatial Resolution [m]	Temporal Resolution [days]	Band	Data Available
Landsat 4 TM	10.40-12.50	120	16	6	1982–1993
Landsat 5 TM	10.40-12.50	120	16	6	1984–2011
Landsat 7 ETM+	10.40-12.50	60	16	6	1999–present
Landsat 8 OLI TIRS	10.60–11.19 11.50–12.50	100	16	10 11	2013–present
Landsat 9 OLI2 TIRS2	10.30–11.30 11.50–12.50	100	16	10 11	2021–present
MODIS Terra	10.78–11.28 11.77–12.27	1000	2	31 32	1999–present
MODIS Aqua	10.78–11.28 11.77–12.27	1000	2	31 32	2002-present
ASTER Terra	8.125–8.475 8.475–8.825 8.925–9.275 10.25–10.95 10.95–11.65	90	2	10 11 12 13 14	1999–present

As presented in Table 1, the most conventional satellite sensors for investigating LSTs include Landsat, the moderate-resolution imaging spectroradiometer (MODIS), and the Advanced Spaceborne Thermal Emission and Reflection Radiometer (ASTER). Several studies have utilized data from polar and/or geostationary satellites, which prioritized the temporal mapping of the studies' regions [30, 31].

Landsat

The Landsat mission began in 1972; however, it took another decade to begin collecting thermal data using Landsat 4 and 5 TMs [14]. TIR radiation is captured by Band 6, which operates day and night (although nighttime observations are often preferred owing to the absence of solar heating) [32]. The instantaneous fields of view for this sensor are 30×30 m in Bands 1–5 and 7 and 120×120 m in Band 6 [33]. Landsat 7 (the ETM+) is comprised of a fixed-scanning multispectral radiometer with eight spectral bands, including a panchromatic band and a thermal band [34]. The spectral resolution of the bands is within the 0.45–12.5 µm range, and its spatial resolution is 30 m (except for Band 6 [60 m – resampled to 30 m] and the panchromatic band [15 m]) [35]. Landsat 8 (the TIRS and operational land imager [OLI]) is comprised of one panchromatic band and eight multispectral bands, with resolutions of 15 m and 30 m, respectively [33]. TIRS is comprised of two thermal bands, with a resolution of 100 m; its data is resampled to 30 m [36].

The authors of [37] employed the Landsat 5 TM and Landsat 8 OLI satellite sensors to determine LU and land cover (LC), LULC, and LST change patterns as well as investigate the impacts of LULC on LST in the Rajshahi City Corporation area in 1999, 2009, and 2019. Also, [38] employed the thermal band potential of the Landsat sensor to monitor the impact of the rural-urban transition on the ecosystem and LST. This study employed LULC classification maps from 1995 to 2016 to evaluate the spatiotemporal dynamics of urbanization at the urban, suburban, sub-rural, and rural levels in Lucknow (the capital of Uttar Pradesh, India) [38]. The authors of [39] employed Landsat's TM and ETM+ to retrieve surface-temperature changes in Egypt during different periods (1990, 2003, 2013, and 2016). The results indicated shifts in LULCs and their correlations with an increases in LSTs [39]. They compared the field data and LST estimations that were obtained by several techniques. Their adoption of valor emissivity and the single-channel equation enhanced the accuracy of the result and brought it closer to the ground-truth temperature [39]. The authors of [40, 41] applied Landsat 5 TM and Landsat 7 ETM+ imagery to environmental and climate studies. These sensors generated spectral bands in the visible (Vis), near-IR (NIR), shortwave IR, and TIR regions [41]. With a wavelength range of 10.4–12.5 µm, the acquired thermal band (Band 6) emitted longwave radiations from the Earth's surface and was conventionally employed for LST estimations [40].

Moderate-Resolution Imaging Spectroradiometer

The MODIS sensor aboard NASA's TERRA/AQUA satellite provides enhanced spatial and spectral resolutions; these enable high-precision high-accuracy measurements of urban thermal environments and ecosystem processes [42]. MODIS is a satellite that collects data from the Earth's surface at regular intervals; it produces outcomes with varying spatial resolutions [32]. MODIS is onboard NASA's Terra (1999) and Aqua (2002) satellites; it exhibits a spectral resolution of 36 bands, which are divided into the Vis, NIR, and IR wavelengths (comprised of Bands 20, 22, 23, 29,

31, and 32, which are centered at 3.79, 3.97, 4.06, 8.55, 11.03, and 12.02 μ m, respectively) [43]. Exhibiting a revisit time of every one or two days, MODIS exhibits low spatial resolutions; Bands 1 and 2, 3–7, and 8–36 exhibit spatial resolutions of 250 m, 500 m, and 1 km, respectively [18]. MODIS sensors can measure the physical and biological properties of the oceans and land as well as the physical properties of the atmosphere [44].

Their thermal data [44] exhibits a resolution of 1 km, thus ensuring the applicability of its products to larger regions. Furthermore, they provide several preprocessed products for users, such as ocean-surface temperatures, ice, snow, evaporation, precipitation, and LST (with daytime and nighttime data), and emissivity, each other from the MOD11C3, MOD11A1, and MOD11A2 products [5]. Sensors with higher temporal resolutions such as the MODIS sensors on the Terra and Aqua satellites can monitor different scales of UHI variations. The eight-day L3 Global 1 km MOD11A2/MYD11A2 SIN Grid LST/emissivity product was used to detect anthropogenic thermal changes and the urban/peri-urban climate [45]. Furthermore, the analysis encompassed several heatwave events, identifying the summers of 2003, 2007, and 2010 as periods of extreme surface-temperature anomalies [46]. The authors of [47] employed the mean surface temperature derived from a series of remote-sensing imagery to examine the spatial and temporal effects of LC zones on LST changes that were observed from the EOS-Aqua-MODIS eight-day product (MYD11A2) for daytime (13:30), with a spatial resolution of 1000 m. They also examined these effects on the environmental, social, and governance (ESG) changes throughout urbanization using the mean ESG values for July and August of both 2005 and 2015 [47]. The high-precision and large area coverage advantages of the MODIS LST data have resulted in their wide adoption in surface UHI studies [13, 48].

Advanced Spaceborne Thermal Emission and Reflection Radiometer

ASTER records images in 14 spectral bands at spatial resolutions of 15, 30, and 90 m for the Vis and NIR bands (Bands 1–3), shortwave IR bands (Bands 4–9), and TIR bands (Bands 10–14), respectively [49]. Daytime and nighttime ASTER data is available, providing significant opportunities to study the diurnal variation of UHI intensities [50]. Attributed to its high spatial and thermal sensitivities, ASTER has been widely deployed for estimating LSTs in urban areas [50].

In a recent study by [49], the authors evaluated LST products that were derived from ASTER imagery driven by a temperature-emissivity separation (TES) algorithm against two independent reference data sets: (a) ASTER LST products (as advanced products that are generated through TES), and (b) Landsat LST data (which has been independently generated by various methods between 1985 and 2017) [49]. The comparison results demonstrated the superiority of ASTER in capturing fine-scale thermal variabilities in urban areas, making it a reliable data source for UHI analysis.

3.2. Algorithms

UHI is based on the correlation with LST, which is determined by processing the thermal bands of satellite images [51]. To compute LST using Landsat, two levels of data (NIR and red bands) from the satellite data must be processed. Landsat Collections Level-1 data can be rescaled to TOA spectral reflectance and/or TOA spectral radiance ($L\lambda$) using the radiometric rescaling coefficients that are provided in the metadata file that is delivered with the Level-1 product. The metadata file also contains the thermal constants for converting the thermal band data to the TOA brightness temperature [52].

The conversion from DN to an $L\lambda$ physical quantity is defined as the radiant flux in each direction considering a surface that is normalized to the surface area and unit solid angle; this is calculated by Equation (1) using the thermal band [53]:

$$L\lambda = M_I Q_{cal} + A_I \tag{1}$$

where: $L\lambda$ – TOA spectral radiance [W/(m²-srad· μ)], M_L – band-specific multiplicative rescaling factor from the metadata (RADIANCE_MULT_BAND_x, where x is the band number), A_L – the band-specific additive rescaling factor from the metadata (RADIANCE_ADD_BAND_x, where x is the band number), and Q_{cal} – the quantized and calibrated standard-product pixel values (DN).

Furthermore, $L\lambda$ is converted into TOA reflectance using the rescaling coefficients in the MTL file following Equation (2) [52]:

$$\rho_{\lambda}' = M_{\rho} Q_{cal} + A_{\rho} \tag{2}$$

where: ρ_{λ}' – TOA spectral radiance [W/(m²-srad· μ)], M_{ρ} – band-specific multiplicative rescaling factor from the metadata (RADIANCE_MULT_BAND_x, where x is the band number), A_{ρ} – the band-specific additive rescaling factor from the metadata (RADIANCE_ADD_BAND_x, where x is the band number), and Q_{cal} – the quantized and calibrated standard-product pixel values (DN).

Thereafter, TOA reflectance with a sun-angle correction for sun illumination is given by Equation (3) [53]:

$$\rho_{\lambda} = \frac{\rho_{\lambda}'}{\cos \theta_{SZ}} = \frac{\rho_{\lambda}'}{\sin \theta_{SE}} \tag{3}$$

where: ρ_{λ} – the TOA planetary reflectance, and θ_{SE} – the local sun elevation angle. The scene-center sun-elevation angle [°] is provided in the metadata (SUN_ELEVATION). Furthermore, θ_{SZ} – the local solar zenith angle, which is given by θ_{SZ} = 90° – θ_{SE} .

The conversion to the TOA brightness temperature [K], proceeds via Equation (4) [53]:

$$BT = \frac{K_2}{\ln\left(\frac{K_1}{L_{\lambda}} + 1\right)} \tag{4}$$

where: BT – the brightness temperature [K], L_{λ} – the TOA spectral radiance [W/(m²-srad·µm)], K_1 – band-specific thermal-conversion constant from the metadata (K1_CONSTANT_BAND_x, where x is the thermal band number), and K_2 – the band-specific thermal-conversion constant from the metadata (K2 CONSTANT_BAND_x, where x is the thermal band number).

Thereafter, the result is converted into temperature [°C] following Equation (5) [54]:

$$BT = BT [K] - 273.15$$
 (5)

The thermal band includes the emissivity (E) of the soil and vegetation. Although the radiance and temperature values can be deduced, including E in the computation is key to generating an LST using the NIR and red bands. Thus, the normalized difference vegetation index (NDVI) is first calculated following Equation (6) [55]:

$$NDVI = \frac{NIRband - REDband}{NIRband + REDband} \tag{6}$$

NDVI is conventionally used to derive the fraction of the vegetation cover (FVC) as expressed in Equation (7) [56]:

$$FVC = \left(\frac{NDVI - NDVI_{bare}}{NDVI_{veg} - NDVI_{bare}}\right)^{2} \tag{7}$$

where $NDVI_{bare}$ and $NDVI_{veg}$ are the NDVI values of the completely bare and fully vegetated pixels, respectively. Following previous studies, both threshold values were set to $NDVI_{bare} = 0.2$ and $NDVI_{veg} = 0.86$; however, several studies have employed $NDVI_{veg} = 0.5$ [56]. The authors of [57] demonstrated that values between 0.8 and 0.9 are more appropriate for realizing high-resolution images. Pixels with NDVI values that are below $NDVI_{bare}$ and above $NDVI_{veg}$ are considered to be completely bare and fully vegetated, respectively.

Thus, the *E* values over vegetated areas at any given time may be derived using the vegetation-cover method, which is defined by Equation (8) [56]:

$$\varepsilon_b = FVC\varepsilon_{b,veg} + (1 - FVC)\varepsilon_{b,bare} \tag{8}$$

where $\varepsilon_{b,veg}$ and $\varepsilon_{b,bare}$ are the emissivities (*Es*) of the vegetation and bare grounds, respectively, for a given spectral band *b*. The *Es* of the vegetated surfaces typically exhibit relatively small variations in the TIR region; therefore, this value is prescribed to $\varepsilon_{pro} = 0.99$.

LST retrieval is realized following [58], as is shown in Equation (9):

$$T_{s} = \frac{BT}{\left(1 + \left(\frac{\lambda BT}{\rho} \cdot \ln \varepsilon\right)\right)} \tag{9}$$

where T_s is LST [K], BT is the at-sensor brightness temperature [K], λ is the wavelength of the emitted radiance (11.5 μ m), ρ is defined as $h \cdot c/k_B = 1.438 \cdot 10^{-2} \text{ m} \cdot \text{K}$ (where: h – Planck's constant, c – the speed of light in a vacuum, k_B – Boltzmann's constant), and ϵ is the spectral surface emissivity.

Several studies have explored the techniques for retrieving LSTs, and three widely utilized methods have emerged: the mono-window algorithm (MWA) by [59], the split-window algorithm (SWA) by [60], and the single-channel (SC) method by [61]. Originally designed for TIR remote sensing in different contexts, these three algorithms must be enhanced when deployed with Landsat 8 TIR data. The authors of [62] developed an improved MWA (IMWA) technique that consolidates on the MWA that was developed in [59], thus allowing for its effective usage with Landsat 8. The MWA that was developed in [59] is expressed in Equation (10). This algorithm requires three parameters: the effective mean atmospheric temperature (T_a), land-surface emissivity (LSE, ϵ), and atmospheric transmittance (τ); however, Equation (10) is proposed for TM images. As the imagery that is employed in this study included Landsat 8 images, this method must be enhanced to make it suitable for new data. The authors of [63] enhanced the algorithm, making it suitable for Band 10 of Landsat 8. This enhanced algorithm is called IMWA and is expressed in Equation (11):

$$T_{s} = \frac{\left[a_{6}(1 - C_{6} - D_{6}) + \left(b_{6}(1 - C_{6} - D_{6}) + C_{6} + D_{6}\right) \cdot T_{6} - D_{6}T_{a}\right]}{C_{6}}$$
(10)

$$T_{s} = \frac{\left[a_{10}(1 - C_{10} - D_{10}) + \left(b_{10}(1 - C_{10} - D_{10}) + C_{10} + D_{10}\right) \cdot T_{10} - D_{10}T_{a}\right]}{C_{10}}$$
(11)

where a_{10} and b_{10} are constants with different values in different temperature ranges (as summarized in Table 2). Furthermore, C_{10} and D_{10} are functions of LSE (ϵ_{10}) and τ (τ_{10}), and the calculation methods are as shown in Equations (4) and (5), respectively (where T_a is the effective mean atmospheric temperature).

SWA was originally proposed by [60]; it is an algorithm for observing the ocean-surface temperature based on AVHRR TIR data and based on the principle that two adjacent TIR bands exhibit different absorption characteristics. The attenuation information of the atmosphere on the thermal radiation can be obtained based on the difference between the brightness temperatures of the two TIR bands (12) [60]:

$$T_c = A_0 + A_1 T_{10} - A_2 T_{11} \tag{12}$$

where T_s is the LST, and T_{10} and T_{11} are the brightness temperatures of Bands 10 and 11, respectively. Furthermore, A_{0} , A_{1} , and A_{2} are the parameters.

The SC method was proposed in 2003 and modified in 2009 by [61]. This algorithm requires only two input parameters: LSE (ϵ), and the atmospheric water vapor content (ω). Differing from MWA, SC does not require the T_a parameter, and the ω must not be calculated to τ . These advantages reduce the error of the final retrieved LST due to the T_a error [61]. Owing to these advantages, the SC algorithm has been adopted by many scholars for various TIR remote sensing, such as Landsat 5 TM, Landsat 7 ETM+, MODIS, ASTER, and ENVISAT AATSR. The authors of [56] optimized the SC method for Landsat 8 and calculated the corresponding parameters using Equation (13):

$$T_{s} = \gamma \left[\frac{1}{\varepsilon} \left(\Psi_{1} L_{sen} + \Psi_{2} \right) + \Psi_{3} \right] + \delta$$
 (13)

where T_s is the LST, ϵ is the LSE, and γ and δ are two parameters depending on the Planck function; they can be calculated. L_{sen} and T_{sen} are the at-sensor registered radiance [W/(m²-sr·µm)] and the at-sensor brightness temperature, respectively. For Band 10 of Landsat 8, b γ = 1324. The atmospheric function parameters are Ψ_1 , Ψ_2 , and Ψ_3 .

For the surface UHI, the UHI intensity is calculated (after identifying the LST) as the temperature difference between the urban and rural areas (Equation (14)) [64]:

$$Surface UHI = ST_{urban} - LST_{rural}$$
 (14)

Urban and rural zones are typically delineated using LC classifications that are derived from the same satellite data set or external products such as GlobeLand30, MODIS LC, or high-resolution maps. Averaging the LST values across each zone enables the spatial and temporal assessments of UHI intensities [65].

3.3. Accuracy

The authors of [37] examined UHI using Landsat image data and support vector machine (SVM) classification based on surface temperatures, with reported

accuracies of 96.86%, 96.15%, and 95.55% in 1999, 2009, and 2019, respectively. The authors of [66] integrated the maximum likelihood classification technique with vegetation-index and surface-temperature algorithms, obtaining accuracies of 94.88%, 93.65%, and 94.82% in 1999, 2009, and 2019, respectively [67].

In China, UHI studies have been conducted using various sensor-algorithm combinations and yielding varying accuracy degrees. The authors of [46] compared the effects of temperature changes between urban and rural areas. Furthermore, the relationship between LST and LU types was investigated at various levels. The results indicated that the five LU types that were retrieved by the object-oriented technique (i.e., vegetation, normal construction land, ultraviolet (UV), water, and unused land) were optimized for further studies, as they demonstrated good accuracy (with an overall accuracy [OA] of 88.70%) [68].

The authors of [69] employed the same LST and NDVI techniques, obtaining kappa coefficients of 0.96 and 0.95 in 1998 and 2009, respectively. The results of the referenced study indicated that optical and thermal remote-sensing techniques could be employed to investigate the environmental characteristics of urban areas. Furthermore, [70] applied the LST algorithm to the observation of elevated heat intensities between 1985 and 2010. To measure landscape patterns and changes more accurately, the researchers employed a novel locally optimized separability enhancement index that was integrated with decision rules (the SEI-DR approach) to solve the classification-accuracy problems (which are characteristic limitations of urbanenvironment studies). This novel SEI-DR approach obtained an OA of 88.00%.

By focusing on several biophysical variables, [71] employed satellite and *in situ* monitoring data to explore the influences of urban development and UHI heatwave occurrences in Romania's Bucharest metropolitan area. Employing the NDVI algorithm, remote-sensing data was obtained from the Landsat TM/ETM+ sensor and MODIS Terra/Aqua time series to assess urban LC/temperature interactions between 2000 and 2016. Overall, the study recorded an OA of 89.00% [45].

The authors of [36] measured LST from Landsat images, demonstrating that the classification accuracy increased when all of the data was added to the original Landsat data. Thus, the overall classification accuracies that were obtained by Landsat 7 ETM+ and Landsat 8 OLI/TIRS were 88.66% and 91.31%, respectively. Moreover, increased urban areas, industries, GHGs, vegetation, irrigated agriculture, and dry agriculture were observed during the study period (13 years), whereas the bare soil and rock areas decreased significantly.

The authors of [72] employed the ESG framework to interpret the UHI phenomena from the different seasons of 2018 in Mashhad, Iran, revealing that the observed UHIs exhibited different behaviors in different seasons regarding location and intensity. Therefore, extracting similar features to the UHIs' behaviors was crucial. The features of the UHI emergence behaviors were analyzed by statistical methods, including principal component analysis (PCA) and fixed multivariate regression. The PCA results indicated that the following four indices were key to studying

UHI emergence: NDVI, the normalized difference built-up index (NDBI), the normalized difference bareness index, and the normalized difference water index. Additionally, these indices could be used to develop a fixed model for examining UHIs across different seasons. Furthermore, the results of the fixed multivariate regression model with different thresholds revealed that it obtained an average OA of 82.15% for the different seasons in Mashhad [72].

Some researchers [4, 16, 39, 44–47, 70–75, 77–93] estimated that the UHIs derived from Landsat using LST algorithms had the levels of accuracy shown in Table 2.

4. Results

Different UHI identification techniques delivered outputs with varying OA levels (Table 2); however, the precision of these methodologies could have been impacted when transferring a method from one area to another, as several variables (including topographical and seasonal fluctuations) might have affected the algorithmic outcomes [76].

Table 2. UHI identification	using remo	te-sensing	technology
	0.00		7000000

Author	Sensor	Algorithm	Accuracy [%]
[77]	Landsat 5 ETM, 7 ETM+, and 8 OLI	LST	OA = 97.00
[39]	Landsat (TM/ETM+/OLI)	LST	OAs: 2002 = 0.87 2011 = 0.85 2021 = 0.92
[78]	Landsat 5 TM Landsat 8	LST	OAs: 1999 = 96.86 2009 = 96.15 2019 = 95.55
[16]	Landsat 5, 7, and 8	LST	Overall Classification Accuracies: Random Forest = 86.41 SVM = 89.93 Multi-Layer Perceptron = 90.28
[79]	Landsat 8	LST	OA = 97.00
[80]	Landsat	LST	OAs: 1995 = 90.00 2005 = 92.00 2016 = 94.00
[81]	Landsat 8	LST	OA = 89.86
[82]	Landsat 8	LST, NDVI	OAs: 1992 = 85.18 2002 = 87.87 2017 = 88.75

Table 2. cont.

Author	Sensor	Algorithm	Accuracy [%]
[83]	Landsat Multispectral: Inland City 1998 = Landsat 5 TM 2000 = Landsat 7 ETM 2007 = Landsat 8 OLI 2015 = OLI Coastal City 1998 = Landsat 5 TM 2000 = Landsat 7 ETM 2007 = Landsat 7 ETM 2015 = Landsat 7 ETM	LST	OAs: Inland City 1998 = 89.87 2000 = 89.44 2007 = 87.78 2015 = 88.33 Coastal City 1998 = 91.56 2000 = 95.56 2007 = 93.33 2015 = 89.44
[84]	Landsat 8	LST, NDBI, NDVI	OAs: 2014 = 82.40 2019 = 84.20
[74]	Landsat 5 TM and Landsat 8 OLI/TIRS	LST	OAs: 1990 = 95.02 2017 = 98.94
[85]	Landsat 5 TM	LST	OAs: Beer Sheva, Israel 1990 = 88.00 2000 = 92.67 2010 = 88.00 Hotan, China 1990 = 93.60 2000 = 89.00 2010 = 90.33 Jodhpur, India 1990 = 82.29 2000 = 80.00 2010 = 82.57
[75]	Landsat images (TM, ETM, and OLI)	LST	OAs: 1990 = 83.67 2003 = 95.65 2013 = 98.04 2016 = 89.59
[70]	Landsat TM and Landsat ETM+	LST	OA = 88.00
[86]	Landsat 5	LST	OAs: 1992 = 88.00 2011 = 89.00
[4]	Landsat's TM and ETM+ imageries	LST, NDVI, NBDI	OAs: 1990 = 91.30 2000 = 86.52 2005 = 87.08 2009 = 98.29

Zuccu zuccu

Table 2. cont.

Landsat 5/4 (TM)	LST, NDVI	OAs: 1990 = 90.40 2009 = 84.40
Landsat 7 ETM and Landsat 5 TM	LST, NDVI	OAs: 1999 = 95.00 2007 = 96.50
Landsat 5	LST	OA = 89.09
Landsat MSS and Landsat TM	LST	OA = 90.00
Landsat 4, 5, 6, 7, and 8	LST, NDVI	OAs: Medan = 98.00 Bandung = 80.00 Makassar = 70.00
Landsat 5, Landsat 8, and MODIS	LST	OA = 88.00
Landsat 5, Landsat 8, and MODIS	LST	OA = 88.00
Landsat 7ETM+, Landsat 8 OLI TIRS, and MODIS	LST, NDVI	City-Based OAs: Colombo 2000 = 80.00 2009 = 83.00 2019 = 90.00 Delhi 2000 = 79.00 2009 = 82.00 2019 = 91.00 Dhaka 2000 = 78.00 2009 = 83.00 2019 = 88.00 Kabul 2000 = 77.00 2009 = 82.00 2019 = 86.00 Karachi 2000 = 79.00 2009 = 86.00 2019 = 86.00 Kathmandu 2000 = 81.00 2009 = 85.00 2019 = 91.00 Thimphu 2000 = 78.00 2009 = 81.00 2019 = 81.00 2019 = 87.00
Aqua-MODIS and Landsat TM/ETM+/OLI	LST	OA: 2005 = 85.03
	Landsat 7 ETM and Landsat 5 TM Landsat 5 Landsat MSS and Landsat TM Landsat 4, 5, 6, 7, and 8 Landsat 5, Landsat 8, and MODIS Landsat 5, Landsat 8, and MODIS Landsat 7ETM+, Landsat 8 OLI TIRS, and MODIS	Landsat 7 ETM and Landsat 5 TM LST Landsat MSS and Landsat TM LST Landsat 4, 5, 6, 7, and 8 LST, NDVI Landsat 5, Landsat 8, and MODIS LST Landsat 5, Landsat 8, and MODIS LST Landsat 7ETM+, Landsat 8 OLI TIRS, and MODIS LST, NDVI

Author	Sensor	Algorithm	Accuracy [%]
[45]	MODIS Terra/Aqua, Landsat TM/ETM+	LST	OA = 89.00
[46]	MODIS, Landsat 5, and Landsat 8	LST	OA = 0.887
[44]	MODIS	LST	Accuracy: ResNet = 0.81 GoogLeNet = 0.85 VGGNet = 0.84 CNN = 0.87
[72]	MODIS	LST	OA = 82.15 Season-Based OAs: Heat = 83.54 Cold = 59.10

Table 2, cont.

Table 2 summarizes the employed satellite sensors and algorithms as well as their observed OAs from remote sensing-driven UHI studies. Generally, Landsat provides time series data and facilitates higher-resolution LST estimations, with OAs ranging from 70.00% to 98.00% (as reported by [16, 73, 77, 83, 91, 93], who applied time series data to LST estimations). The LST method has been widely employed in UHI studies owing to its significance as a key component for realizing energy balance as well as its usefulness as a crucial climatological factor. The LST-estimation technique can accurately enable the identification of the spatial patterns of UHI distributions within different areas. Besides the LST algorithm, a vegetation-index algorithm exists that contributes to the occurrences of UHI phenomena [94].

5. Directions for Future Satellite-Based Urban Heat Island Studies

The authors of [95] recommended that future studies should cover many topics: first, integrating daily satellite thermal data from the Visible Thermal Imager Radiometer Suite data set with *in situ* data from a network of meteorological stations can ease the understanding of the UHI mechanism regarding LULCs; second, future related studies must consider the impact of LULC-type distributions on the emergence of UHIs in urban areas; and third, understanding how human activities and other variables can mitigate the impacts of UHIs on global warming is crucial. To collect LULC data over a period, imagery and preprocessing (including data normalization and time-series-image overlays) are essential [42]. Furthermore, algorithms such as random forest (which rely on computations and the use of training and testing samples) should be used to enhance the LULC-categorization accuracy [96].

Notably, Google Earth Engine (GEE) is garnering attention in environmental and urban studies because of its large collection of geospatial data sets (such as

Landsat and MODIS) [97]. However, ecological and urban developers have encountered three key challenges when using GEE; thus, its full potential cannot be realized in current applications that are limited to simple mapping [91]. Researchers must overcome these technological hurdles by simulating real-world environments via image processing. Furthermore, the review results have revealed that many researchers are unaware of the enhanced geographical-processing capabilities and large geospatial data sets of GEE [98]; thus, its potential to drive ecological and urban modeling remains unexplored. Future studies must aim to enhance GEE performance via specialized tools to model ongoing urban expansions under the UHI effect [42]. As directions for future studies, [98] recommended that remote sensing could be deployed in UHI studies in order to obtain good results with high accuracy. Moreover, Landsat and MODIS satellite imagery can be integrated into UHI studies, as both tools can provide large area coverage with good imaging quality [99]. GEE can also be optimized for long-term UHI studies owing to its criticality [91].

The application of satellites to the study of UHI phenomena has attracted significant interest owing to their capabilities to observe and assess temperature fluctuations in urban areas. We recommend that future satellite-based UHI studies prioritize the following six crucial areas.

5.1. Data Resolution Enhancement

Future satellites must be designed to offer enhanced spatial- and temporal-resolution data, which will facilitate very detailed analyses of low-scale UHI impacts. This advancement might enable researchers to investigate micro-UHIs within cities, thus identifying specific regions that exhibit the most significant heat-related issues [80]. The utilization of remote-sensing-obtained time-series data that is characterized by high geographical resolutions and large temporal coverage is becoming increasingly popular in UHI-related studies [100]. This can be realized by computation, ML, deep-learning (DL), and GEE software applications [101]. Future studies must also focus on exploring techniques for measuring LSTs and LSEs via hyperspectral-TIR, multispectral-temporal, and TIR–microwave data [16]. This study will assess the impacts of aerosols and cirrus clouds. Moreover, the exploration of urban development strategies for mitigating the UHI phenomenon includes an investigation of methods such as enhancing the presence of vegetation and water surfaces.

5.2. Integrating Satellite Data with Ground-Based Sensors

Satellite data provides macrolevel perspectives via thermal imaging and LST measurements, thus enabling the identifications of heat concentrations across large areas [98]. This broad coverage complements high-resolution data that is obtained from ground-based sensors, which capture local environmental factors such

as microscale temperatures and air quality [102]. These sensors are critical for comprehensive analyses of the varying effects of UHIs across different parts of a city. The integration of these data streams can be achieved through advanced data-fusion techniques and ML, which enable the synthesis of multiple data sets into a cohesive analysis framework [51]. Geographic information systems are particularly valuable in this context, as they drive the visual mapping of data from multiple sources, thereby enabling a comprehensive spatial analysis of heat distribution [103]. This integrated approach deepens the understanding of UHI dynamics and improves urban-management strategies toward mitigating the adverse impacts of UHIs on human health and well-being [82]. Furthermore, real-time monitoring and predictive analytics can considerably facilitate predictions of the effects of UHI, thereby enabling timely mitigation actions. Public-engagement platforms can involve the residents of a community and establish feedback channels, thus enhancing the overall effectiveness of monitoring and mitigation efforts [101].

5.3. Artificial Intelligence and Machine Learning

Innovative AI and ML techniques can improve satellite data processing, thereby enabling more-accurate and real-time predictions of UHI effects [104]. Additionally, these technologies can detect relationships and trends that conventional analytic techniques might not be able to promptly recognize. Modeling plays a key role in UHI-phenomenon evaluation – particularly when integrating thermal data from different sensors [105]. ML and AI are garnering increasing attention, and cloud computing platforms such as GEE can significantly impact UHI analyses by efficiently synthesizing big remote-sensing data sets [51]. Thus, the combination of remote-sensing data and station observations in such models is greatly anticipated. Future studies must focus on the effects of UHIs on human health, heat waves, air pollution, and ecological stability.

5.4. Climate Change Modeling

Satellite-based UHI studies can be progressively integrated with climate change models to predict upcoming heat trends in urban areas [104]. This can provide references to urban planners and politicians for the developments of those cities that are more sensitive to climate change effects. Climate models are indispensable tools for studying the complex processes that control global and regional climate changes [42]. An investigation of regional impacts was conducted by developing appropriate temporal- and geographical-scale climate-prediction systems. The existing models exhibit large geographical coverage with limited spatial resolutions. Remotely collected information can be implemented in climate change modeling to analyze the UHI effects in urban and nearby non-urban areas [45]. This integrated approach must feature regional climate models and statistical downscaling models.

5.5. Global Study of Urban Heat Islands

The global study of UHIs is being expanded by the integrations of innovative technologies and approaches for collecting and analyzing data. This methodology can provide useful insights into the influence of urbanization patterns and climatic changes on the impacts of UHIs, completely elucidating their effects in various environments and under various socio-economic conditions [106]. Future studies can identify the common factors that increase heat build-ups in urban areas as well as the different local variables that may impact their intensities and characteristics [84]. This will facilitate the developments of prediction models for the impacts of UHIs under various climate change and urbanization conditions. This will enable the development of more-efficient urban planning strategies. Comparing the impacts of UHIs on public health across different regions may also provide valuable insights for implementing such measures as improved approaches for managing heat waves and increased public-awareness campaigns [10]. The utilization of satellite imagery, ground-based sensors, and projects (including citizen science) will provide a comprehensive data set for predicting patterns and developing global and regional strategies [78]. This method enhances our comprehension of UHIs and strengthens worldwide collaboration among scientists, urban planners, politicians, and the general public, resulting in a more coordinated and efficient response to UHI phenomena [44].

5.6. Urban Heat Islands and Their Impacts

The key terms that were identified from our VOSviewer-based literature review include "Urban Heat Island," "Remote Sensing," and "LST." In 1996, several studies revealed that the UHI phenomenon could intensify the impacts of heat waves by significantly increasing nighttime temperatures [107]. Numerous studies have extensively highlighted the severe implications of global heat crises on public health. In August 2003, Western Europe experienced a significant heat wave that accounted for the deaths of nearly 70,000 people via dehydration, hyperthermia, heat stroke, and respiratory issues [108]. The grid population of the data set was used to analyze the population density owing to the continually changing boundaries of the urban wards, thus proving to be valuable.

An extant UHI study investigated LU and urban redevelopment, emphasizing UV mitigation [46]. The study recommended the accumulation of UV data before 2012 to predict spatiotemporal changes. Moreover, including auxiliary data such as points of interest could increase the accuracy of extracting LU data [46]. Nighttime LSTs may differ regionally from daytime temperatures across cities; this can enable effective urban environmental monitoring and control. Future studies must explore these differences to establish a scientific framework for identifying informal settlements such as slums or UV accumulations. Multi-scale segmentation combined with street data and UV extraction using the nearest-neighbor approach are possible approaches [109].

6. Conclusion

The following conclusions can be deduced from the results of our review and analyses of satellite-based UHI research that started around 1972 through early 2024 by focusing on characteristics based on sensors, algorithms, and accuracy. Moreover, we observed that 1991 was pivotal, marking the integrations of satellite technologies into the development of UHI monitoring and identification systems. From a sensor-based perspective, Landsat and MODIS represent the most frequently deployed platforms for UHI studies. Landsat sensors can be used to observe UHI phenomena - one of which is the thermal band that is detected on the Landsat satellite (Landsat 8 consists of Bands 10 and 11). Furthermore, MODIS sensor, as its frequent temporal resolution effectively enables the studies of temporal variations in UHI such as diurnal, seasonal, and decadal variations. Moreover, satellite sensors can be selected based on the research time. Regarding the algorithms, the land surface temperature (LST) indicator and normalized difference vegetation index (NDVI) were the most deployed algorithms. Regarding accuracy, the integrations of satellite sensors and algorithms into UHI studies provide a promising range of accuracies. When conducting UHI studies, algorithms must be selected based on the specific characteristics of the study location and the data-collection period in order to obtain reliable and accurate results.

The future of satellite-based UHI monitoring is promising, with technological advancements driving the developments of effective techniques such as data fusion, gap filling, ML, and DL to enhance UHI monitoring. Adopting models that combine data from many sensors and fill in missing information might enhance UHI monitoring by utilizing a comprehensive time series of thermal data with high spatial detail. These methods produce time-dense high-resolution UHI data over prolonged periods by combining data from other sensors. ML has gained attention in UHI studies; however, its applicability is limited to the predictions of phenomena in the natural environment. GEE is a cloud-based platform for large-scale geospatial analysis. It enables various geographical-scale UHI assessments, including local, regional, and global scale assessments.

Finally, future directions indicate that satellite-based UHI studies should prioritize six crucial points: enhanced data resolution, satellite data integration with ground-based sensors, AI and ML, climate change modeling, global UHI studies, and UHIs and their impacts.

Funding

This research was funded by The Ministry of Education and Culture with the scheme from the National Research Priority with Contract No. 106/E5/PG.02.00. PL/2024 and 328/B.005/LPPM/ITENAS/VI/2024.

CRediT Author Contribution

- S. D.: conceptualization, methodology, writing review and editing, formal analysis, formal analysis, supervision, validation, funding acquisition.
- R. H.: methodology, original draft preparation, writing review and editing, formal analysis, validation, data curation, project administration.
 - S. R.: software, visualization, original draft preparation, data curation.

Declaration of Competing Interest

The authors declare that they have no known competing financial interests or personal relationships that could have appeared to influence the work that is reported in this paper.

Data Availability

No data.

Use of Generative AI and AI-Assisted Technologies

No generative AI or AI-assisted technologies were employed in the preparation of this manuscript

Acknowledgements

We would like to thank to The Ministry of Education and Culture and LPPM Itenas Bandung for grant No 106/E5/PG.02.00.PL/2024 and No 328/B.005/LPPM/ITE-NAS/VI/2024.

References

- [1] Oke T.R.: *The energetic basis of the urban heat island*. Quarterly Journal of the Royal Meteorological Society, vol. 108(455), 1982, pp. 1–24. https://doi.org/10.1002/qj.49710845502.
- [2] Voogt J.A., Oke T.R.: *Thermal remote sensing of urban climates*. Remote Sensing of Environment, vol. 86(3), 2003, pp. 370–384. https://doi.org/10.1016/S0034-4257(03)00079-8.
- [3] Wang S., Ma Q., Ding H., Liang H.: *Detection of urban expansion and land surface temperature change using multi-temporal Landsat images*. Resources, Conservation and Recycling, vol. 128, 2018, pp. 526–534. https://doi.org/10.1016/j.resconrec.2016.05.011.
- [4] Xiong Y., Huang S., Chen F., Ye H., Wang C., Zhu C.: *The impacts of rapid urbanization on the thermal environment: A remote sensing study of Guangzhou, South China*. Remote Sensing, vol. 4(7), 2012, pp. 2033–2056. https://doi.org/10.3390/rs4072033.
- [5] Imhoff M.L., Zhang P., Wolfe R.E., Bounoua L.: Remote sensing of the urban heat island effect across biomes in the continental USA. Remote Sensing of Environment, vol. 114(3), 2010, pp. 504–513. https://doi.org/10.1016/j.rse.2009.10.008.

- [6] MetLink Royal Meteorological Society: *Urban Heat Islands*. 2013. https://www.metlink.org/fieldwork-resource/urban-heat-island-introduction/ [access: 27.06.2024].
- [7] Pal S., Ziaul S.: Detection of land use and land cover change and land surface temperature in English Bazar urban centre. Egyptian Journal of Remote Sensing and Space Science, vol. 20(1), 2017, pp. 125–145. https://doi.org/10.1016/j.ejrs.2016.11.003.
- [8] Tosca M.G., Campbell J., Garay M., Lolli S., Seidel F.C., Marquis J., Kalashniko-va O.: Attributing accelerated summertime warming in the southeast United States to recent reductions in aerosol burden: Indications from vertically-resolved observations. Remote Sensing, vol. 9(7), 2017, 674. https://doi.org/10.3390/rs9070674.
- [9] IPCC: Global Warming of 1.5°C: Headline Statements from the Summary for Policymakers, [in:] Global Warming of 1.5°C: An IPCC Special Report on the impacts of global warming of 1.5°C above pre-industrial levels and related global greenhouse gas emission pathways, in the context of strengthening the global response to the threat of climate change, 2018, pp. 1–2.
- [10] Zhou D., Xiao J., Bonafoni S., Berger C., Deilami K., Zhou Y., Frolking S., Yao R., Qiao Z., Sobrino J.A.: *Satellite remote sensing of surface urban heat islands: Progress, challenges, and perspectives.* Remote Sensing, vol. 11(1), 2019, 48. https://doi.org/10.3390/rs11010048.
- [11] Na N., Xu D., Fang W., Pu Y., Liu Y., Wang H.: Automatic detection and dynamic analysis of urban heat islands based on Landsat images. Remote Sensing, vol. 15(16), 2023, 4006. https://doi.org/10.3390/rs15164006.
- [12] Carmin J., Nadkarni N., Rhie C.: *Progress and Challenges in Urban Climate Adaptation Planning: Results of a Global Survey*. MIT, Cambridge 2012. https://www.cakex.org/sites/default/files/documents/Urban_Adaptation_Report_23May2012.pdf [access: 21.05.2023].
- [13] Duncan J.M.A., Boruff B., Saunders A., Sun Q., Hurley J., Amati M.: *Turning down the heat: An enhanced understanding of the relationship between urban vegetation and surface temperature at the city scale*. Science of the Total Environment, vol. 656, 2019, pp. 118–128. https://doi.org/10.1016/j.scitotenv.2018.11.223.
- [14] Soux A., Voogt J.A., Oke T.R.: *A model to calculate what a remote sensor "sees" of an urban surface*. Boundary-Layer Meteorology, vol. 112(2), 2004, pp. 109–132. https://doi.org/10.1023/B:BOUN.0000027978.21230.b7.
- [15] Yuan Y., Santamouris M., Xu D., Geng X., Li C., Cheng W., Su L., Xiong P., Fan Z., Wang X., Liao C.: *Surface urban heat island effects intensify more rapidly in lower income countries*. npj Urban Sustainability, vol. 5, 2025, 11. https://doi.org/10.1038/s42949-025-00198-9.
- [16] Tepanosyan G., Muradyan V., Hovsepyan A., Pinigin G., Medvedev A., Asmaryan S.: Studying spatial-temporal changes and relationship of land cover and surface Urban Heat Island derived through remote sensing in Yerevan, Armenia. Building and Environment, vol. 187, 2021, 107390. https://doi.org/10.1016/j.buildenv.2020.107390.

- [17] Weng Q., Larson R.C.: Satellite remote sensing of urban heat islands: Current practice and prospects, [in:] Jensen R.R., Gatrell J.D., McLean D.D. (eds.), Geo-Spatial Technologies in Urban Environments: Policy, Practice, and Pixels, Springer, Berlin, Heidelberg 2005, pp. 91–111. https://doi.org/10.1007/3-540-26676-3 10.
- [18] Frey C.M., Kuenzer C.: *Analysing a 13 years MODIS land surface temperature time series in the Mekong Basin,* [in:] Kuenzer C., Dech S., Wagner W. (eds.), *Remote Sensing Time Series: Revealing Land Surface Dynamics,* Remote Sensing and Digital Image Processing, vol. 22, Springer, Cham 2015, pp. 119–140. https://doi.org/10.1007/978-3-319-15967-6_6.
- [19] Nill L., Ullmann T., Kneisel C., Sobiech-Wolf J., Baumhauer R.: Assessing spatiotemporal variations of Landsat land surface temperature and multispectral indices in the Arctic Mackenzie Delta region between 1985 and 2018. Remote Sensing, vol. 11(19), 2019, 2329. https://doi.org/10.3390/rs11192329.
- [20] Wan Z., Dozier J.: Viewing-angle dependent split-window method for retrieving land-surface temperatures from space, [in:] Proceedings of the International Geoscience and Remote Sensing Symposium (IGARSS), IEEE, 1995, pp. 1665–1667. https://doi.org/10.1109/IGARSS.1995.521176.
- [21] Tian L., Li Y., Lu J., Wang J.: Review on urban heat island in China: Methods, its impact on buildings energy demand and mitigation strategies. Sustainability, vol. 13(2), 2021, 762. https://doi.org/10.3390/su13020762.
- [22] Yang C., Wu G., Chen J., Li Q., Ding K., Wang G., Zhang C.: Simulating and forecasting spatio-temporal characteristic of land-use/cover change with numerical model and remote sensing: A case study in Fuxian Lake Basin, China. European Journal of Remote Sensing, vol. 52(1), 2019, pp. 374–384. https://doi.org/10.1080/22797254.2019.1611387.
- [23] Ramakreshnan L., Aghamohammadi N., Fong C.S., Ghaffarianhoseini A., Ghaffarianhoseini A., Wong L.P., Hassan N., Sulaiman N.M.: *A critical review of urban heat island phenomenon in the context of Greater Kuala Lumpur, Malaysia*. Sustainable Cities and Society, vol. 39, 2018, pp. 99–113. https://doi.org/10.1016/j.scs.2018.02.005.
- [24] Pahlevan-Sharif S., Mura P., Wijesinghe S.N.R.: *A systematic review of systematic reviews in tourism*. Journal of Hospitality and Tourism Management, vol. 39, 2019, pp. 158–165. https://doi.org/10.1016/j.jhtm.2019.04.001.
- [25] Hernawati R., Wikantika K., Darmawan S.: Modeling of oil palm phenology based on remote sensing data: Opportunities and challenges. Journal of Applied Remote Sensing, vol. 16(2), 2022, 021501. https://doi.org/10.1117/1. jrs.16.021501.
- [26] Bustos Navarrete C., Morales Malverde M.G., Salcedo Lagos P., Díaz Mujica A.: *Buhos: A web-based systematic literature review management software*. SoftwareX, vol. 7, 2018, pp. 360–372. https://doi.org/10.1016/j.softx.2018.10.004.

- [27] Popay J., Roberts H., Sowden A., Petticrew M., Britten N., Arai L., Roen K., Rodgers M.: *Developing guidance on the conduct of narrative synthesis in systematic reviews*. Journal of Epidemiology and Community Health, vol. 59 (Suppl. 1), 2005, A7.
- [28] Ngie A., Abutaleb K., Ahmed F., Darwish A., Ahmed M.: *Assessment of urban heat island using satellite remotely sensed imagery: A review.* South African Geographical Journal, vol. 96(2), 2014, pp. 198–214. https://doi.org/10.1080/03736245.2014.924864.
- [29] Saleem M.S., Ahmad S.R., Shafiq-Ur-Rehman, Javed M.A.: *Impact assessment of urban development patterns on land surface temperature by using remote sensing techniques: A case study of Lahore, Faisalabad and Multan district.* Environmental Science and Pollution Research, vol. 27(32), 2020, pp. 39865–39878. https://doi.org/10.1007/s11356-020-10050-5.
- [30] Freitas S.C., Trigo I.F., Macedo J., Barroso C., Silva R., Perdigão R.: *Land surface temperature from multiple geostationary satellites*. International Journal of Remote Sensing, vol. 34(9–10), 2013, pp. 3051–3068. https://doi.org/10.1080/01431161.2012.716925.
- [31] Almeida J., dos Santos J.A., Alberton B., Torres R.D.S., Morellato L.P.C.: *Remote phenology: Applying machine learning to detect phenological patterns in a cerrado savanna*, [in:] 2012 IEEE 8th International Conference on E-Science (e-Science), IEEE, 2012, pp. 1–8. https://doi.org/10.1109/eScience.2012.6404438.
- [32] Wang M., Zhang Z.Z., Hu T., Wang G., He G., Zhang Z.: An efficient framework for producing Landsat-based land surface temperature data using Google Earth Engine. IEEE Journal of Selected Topics in Applied Earth Observations and Remote Sensing, vol. 13, 2020, pp. 4689–4701. https://doi.org/10.1109/JSTARS.2020.3014586.
- [33] Dewa D.D., Buchori I.: Impacts of rapid urbanization on spatial dynamics of land use-based carbon emission and surface temperature changes in the Semarang Metropolitan Region, Indonesia. Environmental Monitoring and Assessment, vol. 195(2), 2023, 259. https://doi.org/10.1007/s10661-022-10839-6.
- [34] Tariq A., Shu H.: *CA-Markov chain analysis of seasonal land surface temperature and land use land cover change using optical multi-temporal satellite data of Faisalabad, Pakistan*. Remote Sensing, vol. 12(20), 2020, 3402. https://doi.org/10.3390/rs12203402.
- [35] Deilami K., Kamruzzaman M., Liu Y.: *Urban heat island effect: A systematic review of spatio-temporal factors, data, methods, and mitigation measures.* International Journal of Applied Earth Observation and Geoinformation, vol. 67, 2018, pp. 30–42. https://doi.org/10.1016/j.jag.2017.12.009.
- [36] Aslan N., Koc-San D.: Analysis of relationship between urban heat island effect and land use/cover type using Landsat 7 ETM+ and Landsat 8 OLI images. International Archives of the Photogrammetry, Remote Sensing and Spatial Information Sciences – ISPRS Archives, vol. XLI-B8, 2016, pp. 821–828. https://doi.org/10.5194/isprs-archives-XLI-B8-821-2016.

- [37] Al Kafy A., Al Faisal A., Shuvo R.M., Naim M.N.H., Sikdar M.S., Chowdhury R.R., Islam M.A., Sarker M.H.S., Khan M.H.H., Kona M.A.: Remote sensing approach to simulate the land use/land cover and seasonal land surface temperature change using machine learning algorithms in a fastest-growing megacity of Bangladesh. Remote Sensing Applications: Society and Environment, vol. 21, 2021, 100463. https://doi.org/10.1016/j.rsase.2020.100463.
- [38] Shukla S.S., Jaiswal V.: *Applicability of artificial intelligence in different fields of life.* International Journal of Scientific Engineering and Research (IJSER), vol. 1(1), 2013, pp. 28–35. https://www.doi.org/10.70729/1130915.
- [39] Moazzam M.F.U., Doh Y.H., Lee B.G.: *Impact of urbanization on land surface temperature and surface urban heat island using optical remote sensing data: A case study of Jeju Island, Republic of Korea.* Building and Environment, vol. 222, 2022, 109368. https://doi.org/10.1016/j.buildenv.2022.109368.
- [40] Li Z.L., Tang B.H., Wu H., Ren H., Yan G., Wan Z., Trigo I.F., Sobrino J.A.: Satellite-derived land surface temperature: Current status and perspectives. Remote Sensing of Environment, vol. 131, 2013, pp. 14–37. https://doi.org/10.1016/ j.rse.2012.12.008.
- [41] Wan Z., Wang P., Li X.: Using MODIS land surface temperature and normalized difference vegetation index products for monitoring drought in the southern Great Plains, USA. International Journal of Remote Sensing, vol. 25(1), 2004, pp. 61–72. https://doi.org/10.1080/0143116031000115328.
- [42] Almeida C.R., de, Furst L., Gonçalves A., Teodoro A.C.: *Remote sensing image-based analysis of the urban heat island effect in Bragança, Portugal.* Environments, vol. 9(8), 2022, 98. https://doi.org/10.3390/environments9080098.
- [43] Neumann W., Martinuzzi S., Estes A.B., Pidgeon A.M., Dettki H., Ericsson G., Radeloff V.C.: *Opportunities for the application of advanced remotely-sensed data in ecological studies of terrestrial animal movement*. Movement Ecology, vol. 3(1), 2015, 8. https://doi.org/10.1186/s40462-015-0036-7.
- [44] Khalil U., Aslam B., Azam U., Khalid H.M.D. *Time series analysis of land surface temperature and drivers of urban heat island effect based on remotely sensed data to develop a prediction model.* Applied Artificial Intelligence, vol. 35(15), 2021, pp. 1803–1828. https://doi.org/10.1080/08839514.2021.1993633.
- [45] Zoran M.A., Savastru R., Savastru D., Tautan M.N., Penache A.C.: Spatiotemporal changes of urban land surface albedo impact on thermal environment in Bucharest Metropolitan City. WSEAS Transactions on Environment and Development, vol. 19, 2023, pp. 1037–1044. https://doi.org/10.37394/232015. 2023.19.98
- [46] Wu W., Ren H., Yu M., Wang Z.: Distinct influences of urban villages on urban heat islands: A case study in the Pearl River Delta, China. International Journal of Environmental Research and Public Health, vol. 15(8), 2018, 1666. https://doi.org/10.3390/ijerph15081666.

- [47] Lu Y., Yang J., Ma S.: Dynamic changes of local climate zones in the Guang-dong-Hong Kong-Macao Greater Bay Area and their spatio-temporal impacts on the surface urban heat island effect between 2005 and 2015. Sustainability, vol. 13(11), 2021, 6374. https://doi.org/10.3390/su13116374.
- [48] Li Z.-L., Si M., Leng P.: Review of remotely sensed surface urban heat islands from the fresh perspective of comparisons among different regions. Progress in Electromagnetics Research C, vol. 102, 2020, pp. 31–46. https://doi.org/10.2528/PIERC20020403.
- [49] Parastatidis D., Mitraka Z., Chrysoulakis N., Abrams M.: *Online global land surface temperature estimation from Landsat*. Remote Sensing, vol. 9(12), 2017, 1208. https://doi.org/10.3390/rs9121208.
- [50] Abrams M., Tsu H., Hulley G., Iwao K., Pieri D., Cudahy T., Kargel J.: The Advanced Spaceborne Thermal Emission and Reflection Radiometer (ASTER) after fifteen years: Review of global products. International Journal of Applied Earth Observation and Geoinformation, vol. 38, 2015, pp. 292–301. https://doi.org/ 10.1016/j.jag.2015.01.013.
- [51] Addas A.: Machine learning techniques to map the impact of urban heat island: Investigating the city of Jeddah. Land, vol. 12(6), 2023, 1159. https://doi.org/10.3390/land12061159.
- [52] Vermote E., Roger J.C., Franch B., Skakun S.: LASRC (Land SurReflectance Code): Overview, application and validation using MODIS, VIIRS, LANDSAT and Sentinel 2 data's, [in:] 2018 IEEE International Geoscience & Remote Sensing Symposium: Proceedings: July 22–27, 2018, Valencia, Spain, IEEE, Piscataway 2018, pp. 8173–8176. https://doi.org/10.1109/IGARSS.2018.8517622.
- [53] USGS (United States Geological Survey): *Using the USGS Landsat Level-1 Data Product.* https://www.usgs.gov/landsat-missions/using-usgs-landsat-level-1-data-product [access: 2.07.2024].
- [54] Fashae O., Adagbasa E., Olusola A., Obateru R.: Land use/land cover change and land surface temperature of Ibadan and environs, Nigeria. Environmental Monitoring and Assessment, vol. 192, 2020, 109. https://doi.org/10.1007/ s10661-019-8054-3.
- [55] Kumari B., Tayyab M., Shahfahad, Salman, Mallick J., Khan M.F., Rahman A.: Satellite-driven land surface temperature (LST) using Landsat 5, 7 (TM/ETM+ LC) and Landsat 8 (OLI/TIRS) data and its association with built-up and green cover over urban Delhi, India. Remote Sensing in Earth Systems Sciences, vol. 1(3–4), 2018, pp. 63–78. https://doi.org/10.1007/s41976-018-0004-2.
- [56] Jiménez-Muñoz J.C., Sobrino J.A., Skoković D., Mattar C., Cristóbal J.: Land surface temperature retrieval methods from Landsat-8 thermal infrared sensor data. IEEE Geoscience and Remote Sensing Letters, vol. 11(10), 2014, pp. 1840–1843. https://doi.org/10.1109/LGRS.2014.2312032.
- [57] Karnieli A., Ohana-Levi N., Silver M., Paz-Kagan T., Panov N., Varghese D., Chrysoulakis N., Provenzale A.: Spatial and seasonal patterns in vegetation

- growth-limiting factors over Europe. Remote Sensing, vol. 11(20), 2019, 2406. https://doi.org/10.3390/rs11202406.
- [58] Stathopoulou M., Cartalis C.: Daytime urban heat islands from Landsat ETM+ and Corine land cover data: An application to major cities in Greece. Solar Energy, vol. 81(3), 2007, pp. 358–368. https://doi.org/10.1016/j.solener.2006.06.014.
- [59] Qin Z., Karnieli A., Berliner P.: *A mono-window algorithm for retrieving land surface temperature from Landsat TM data and its application to the Israel–Egypt border region.* International Journal of Remote Sensing, vol. 22(18), 2001, pp. 3719–3746. https://doi.org/10.1080/01431160010006971.
- [60] McMillin L.M.: Estimation of sea surface temperatures from two infrared window measurements with different absorption. Journal of Geophysical Research, vol. 80(36), 1975, pp. 5113–5117. https://doi.org/10.1029/JC080i036p05113.
- [61] Jiménez-Muñoz J.C., Sobrino J.A.: A generalized single-channel method for retrieving land surface temperature from remote sensing data. Journal of Geophysical Research: Atmospheres, vol. 108(D22), 2003, 4688. https://doi.org/10.1029/2003JD003480.
- [62] Wang L., Lu Y., Yao Y.: Comparison of three algorithms for the retrieval of land surface temperature from Landsat 8 images. Sensors, vol. 19(22), 2019, 5049. https://doi.org/10.3390/s19225049.
- [63] Wang F., Qin Z., Song C., Tu L., Karnieli A., Zhao S.: *An improved mono-window algorithm for land surface temperature retrieval from Landsat 8 Thermal Infrared Sensor data.* Remote Sensing, vol. 7(4), 2015, pp. 4268–4289. https://doi.org/10.3390/rs70404268.
- [64] Sismanidis P., Bechtel B., Perry M., Ghent D.: *The seasonality of surface urban heat islands across climates*. Remote Sensing, vol. 14(10), 2022, 2318. https://doi.org/10.3390/rs14102318.
- [65] Vallet A., Dupuy S., Verlynde M., Gaetano R.: *Generating high-resolution land use and land cover maps for the greater Mariño watershed in 2019 with machine learning*. Scientific Data, vol. 11, 2024, 915. https://doi.org/10.1038/s41597-024-03750-x.
- [66] Kafy A.-A., Rahman M.S., Faisal A.-A., Hasan M.M., Islam M.: *Modelling future land use land cover changes and their impacts on land surface temperatures in Rajshahi, Bangladesh.* Remote Sensing Applications: Society and Environment, vol. 18, 2020, 100314. https://doi.org/10.1016/j.rsase.2020.100314.
- [67] Kafy A.-A., Faisal A.-A., Rahman M.S., Islam M., Al Rakib A., Islam M.A., Khan M.H.H., Sikdar M.S., Sarker M.H.S., Mawa J., Sattar G.S.: *Prediction of seasonal urban thermal field variance index using machine learning algorithms in Cumilla, Bangladesh.* Sustainable Cities and Society, vol. 64, 2021, 102542. https://doi.org/10.1016/j.scs.2020.102542.
- [68] Wang M., He G., Zhang Z., Wang G., Wang Z., Yin R., Cui S., Wu Z., Cao X.: A radiance-based split-window algorithm for land surface temperature retrieval: Theory and application to MODIS data. International Journal of Applied Earth Observation and Geoinformation, vol. 76, 2019, pp. 204–217. https://doi.org/ 10.1016/j.jag.2018.11.015.

- [69] Zareie S., Khosravi H., Nasiri A., Dastorani M.: *Using Landsat Thematic Mapper (TM) sensor to detect change in land surface temperature in relation to land use change in Yazd, Iran.* Solid Earth, vol. 7(6), 2016, pp. 1551–1564. https://doi.org/10.5194/se-7-1551-2016.
- [70] Feyisa G.L., Meilby H., Jenerette G.D., Pauliet S.: Locally optimized separability enhancement indices for urban land cover mapping: Exploring thermal environmental consequences of rapid urbanization in Addis Ababa, Ethiopia. Remote Sensing of Environment, vol. 175, 2016, pp. 14–31. https://doi.org/10.1016/j.rse.2015.12.026.
- [71] Zoran M.A., Savastru R.S., Savastru D.M., Dida A.: Impacts of urban growth and heat waves events on the urban heat island in Bucharest city, [in:] Remote Sensing Technologies and Applications in Urban Environments, Proceedings of SPIE, vol. 10008, SPIE, 2016, 1000813. https://doi.org/10.1117/12.2241360.
- [72] Nanjam R., Farnood Ahmadi F.: A new spatiotemporal model for analyzing the variations of urban heat islands using remotely sensed multi spectral images: The case of Mashhad City, Iran. Journal of the Indian Society of Remote Sensing, vol. 49(10), 2021, pp. 2489–2502. https://doi.org/10.1007/s12524-021-01404-8.
- [73] Kayet N., Pathak K., Chakrabarty A., Sahoo S.: *Urban heat island explored by co-relationship between land surface temperature vs multiple vegetation indices*. Spatial Information Research, vol. 24(5), 2016, pp. 515–529. https://doi.org/10.1007/s41324-016-0049-3.
- [74] Le M.T., Bakaeva N.: A technique for generating preliminary satellite data to evaluate SUHI using cloud computing: A case study in Moscow, Russia. Remote Sensing, vol. 15(13), 2023, 3294. https://doi.org/10.3390/rs15133294.
- [75] Kafy A.-A., Faisal A.-A., Rahman M.S., Islam M., Rakib A.-A., Islam M.A., Khan M.H.H., Sikdar M.S., Sarker M.H.S., Mawa J., Sattar G.S.: *Prediction of seasonal urban thermal field variance index using machine learning algorithms in Cumilla, Bangladesh.* Sustainable Cities and Society, vol. 64, 2021, 102542. https://doi.org/10.1016/j.scs.2020.102542.
- [76] Verma P., Raghubanshi A.S., Srivastava P.K., Raghubanshi A.S.R.: *Appraisal of kappa-based metrics and disagreement indices of accuracy assessment for parametric and nonparametric techniques used in LULC classification and change detection.* Modeling Earth Systems and Environment, vol. 6(2), 2020, pp. 1045–1059. https://doi.org/10.1007/s40808-020-00740-x.
- [77] Shukla A., Jain K.: *Critical analysis of rural-urban transitions and transformations in Lucknow city, India.* Remote Sensing Applications: Society and Environment, vol. 13, 2019, pp. 445–456. https://doi.org/10.1016/j.rsase.2019.01.001.
- [78] Mushore T.D., Dube T., Manjowe M., Gumindoga W., Chemura A., Rousta I., Odindi J., Mutanga O.: Remotely sensed retrieval of local climate zones and their linkages to land surface temperature in Harare metropolitan city, Zimbabwe. Urban Climate, vol. 27, 2019, pp. 259–271. https://doi.org/10.1016/j.uclim.2018.12.006.

- [79] Chaka D.S., Oda T.K.: *Understanding land surface temperature on rift areas to examine the spatial variation of urban heat island: The case of Hawassa, southern Ethiopia*. GeoJournal, vol. 86(2), 2021, pp. 993–1014. https://doi.org/10.1007/s10708-019-10110-5.
- [80] Tarawally M., Xu W., Hou W., Mushore T.D.: Comparative analysis of responses of land surface temperature to long-term land use/cover changes between a coastal and inland city: A case of Freetown and Bo Town in Sierra Leone. Remote Sensing, vol. 10(1), 2018, 112. https://doi.org/10.3390/rs10010112.
- [81] Hernawati R., Darmawan S., Cahyanto D.: The impact of built-up area on land surface temperature derived from cloud-computing Landsat 8 imagery, [in:] Proceedings of the International Conference on Green Technology and Design (ICGTD), vol. 2020, IEEE, 2020, pp. 46–51.
- [82] Nurwanda A.: *City expansion and urban heat island in Bogor*. IOP Conference Series: Earth and Environmental Science, vol. 179, 2018, 012007. https://doi.org/10.1088/1755-1315/179/1/012007.
- [83] Fan C., Myint S.W., Kaplan S., Middel A., Zheng B., Rahman A., Huang H.-P., Brazel A., Blumberg D.G.: Understanding the impact of urbanization on surface urban heat islands – a longitudinal analysis of the oasis effect in subtropical desert cities. Remote Sensing, vol. 9(7), 2017, 672. https://doi.org/10.3390/rs9070672.
- [84] El-Zeiny A.M., Effat H.A.: Environmental monitoring of spatiotemporal change in land use/land cover and its impact on land surface temperature in El-Fayoum governorate, Egypt. Remote Sensing Applications: Society and Environment, vol. 8, 2017, pp. 266–277. https://doi.org/10.1016/j.rsase.2017.10.003.
- [85] Meng F., Liu M.: *Remote-sensing image-based analysis of the patterns of urban heat islands in rapidly urbanizing Jinan, China*. International Journal of Remote Sensing, vol. 34(24), 2013, pp. 8838–8853. https://doi.org/10.1080/01431161. 2013.853895.
- [86] Sharma R., Ghosh A., Joshi P.K.: Spatio-temporal footprints of urbanisation in Surat, the Diamond City of India (1990–2009). Environmental Monitoring and Assessment, vol. 185(4), 2013, pp. 3313–3325. https://doi.org/10.1007/s10661-012-2792-9.
- [87] Tan K.C., Lim H.S., MatJafri M.Z., Abdullah K.: Landsat data to evaluate urban expansion and determine land use/land cover changes in Penang Island, Malaysia. Environmental Earth Sciences, vol. 60(7), 2010, pp. 1509–1521. https://doi.org/10.1007/s12665-009-0286-z.
- [88] Sun C.Y., Kato S., Gou Z.: Application of low-cost sensors for urban heat island assessment: A case study in Taiwan. Sustainability, vol. 10(11), 2019, 2759. https://doi.org/10.3390/su11102759.
- [89] Lo C.-P.: Mapping Atlanta's land use/cover change and its impact on the environment using time sequential Landsat images. International Archives of Photogrammetry and Remote Sensing, vol. XXXIII (part B7), 2000, pp. 790–796.

- [90] Hernawati R., Darmawan S.: The investigation of land surface temperature and vegetation in big cities of Indonesia, [in:] 44th Asian Conference on Remote Sensing (ACRS 2023), 30 October 3 November 2023, Taipei, Taiwan, Curran Associates, Inc., Red Hook, NY, pp. 1149–1162
- [91] Hassan T., Zhang J., Prodhan F.A., Khorshed A.K.M., Dewan A., Hassan Q.K.: Surface urban heat islands dynamics in response to LULC and vegetation across South Asia (2000–2019). Remote Sensing, vol. 13(16), 3177. https://doi.org/10.3390/rs13163177.
- [92] Tariq A., Riaz I., Ahmad Z., Yang B., Amin M., Kausar R., Andleeb S., Farooqi M.A., Rafiq M.: Land surface temperature relation with normalized satellite indices for the estimation of spatio-temporal trends in temperature among various land use land cover classes of an arid Potohar region using Landsat data. Environmental Earth Sciences, vol. 79(19), 2020, 681. https://doi.org/10.1007/s12665-019-8766-2.
- [93] Mishra K., Garg R.D.: Assessing variations in land cover-land use and surface temperature dynamics for Dehradun, India, using multi-time and multi-sensor landsat data. Environmental Monitoring and Assessment, vol. 195, 2023, 373. https://doi.org/10.1007/s10661-023-10945-z.
- [94] Naf M.Z.T., Hernawati R.: Analisis fenomena UHI (Urban Heat Island) berdasar-kan hubungan antara kerapatan vegetasi dengan suhu permukaan (Studi kasus: Kota Bandung, Jawa Barat) [Analysis of the Urban Heat Island (UHI) phenomenon based on the relationship between vegetation density and land surface temperature (Case study: Bandung City, West Java)]. ITB Indonesian Journal of Geospatial, vol. 5(1), 2018, pp. 25–36.
- [95] Meng F., Shan B., Liu M.: Remote-sensing evaluation of the relationship between urban heat islands and urban biophysical descriptors in Jinan, China. Journal of Applied Remote Sensing, vol. 8(1), 2014, 083693. https://doi.org/10.1117/1.JRS.8.083693.
- [96] Goldblatt R., Addas A., Crull D., Crommelinck S., Elhag M., Johannsen F., Müller J., Poortinga A., Schellinger J., Syrris V., Thiel M.: Remotely sensed derived land surface temperature (LST) as a proxy for air temperature and thermal comfort at a small geographical scale. Land, vol. 10(4), 2021, 410. https://doi.org/10.3390/land10040410.
- [97] Gorelick N., Hancher M., Dixon M., Ilyushchenko S., Thau D., Moore R.: *Google Earth Engine: Planetary-scale geospatial analysis for everyone.* Remote Sensing of Environment, vol. 202, 2017, pp. 18–27. https://doi.org/10.1016/j.rse.2017.06.031.
- [98] Kumar L., Mutanga O.: Google Earth Engine applications since inception: Usage, trends, and potential. Remote Sensing, vol. 10(10), 2018, 1509. https://doi.org/10.3390/rs10101509.

- [99] Pertuack S., Latue P.C.: Geographic artificial intelligence and unmanned aerial vehicles application for correlation analysis of settlement density and land surface temperature in Panggang Island Jakarta. Buana Jurnal Geografi, Ekologi dan Kebencanaan, vol. 1(1), 2023, pp. 39–47. https://doi.org/10.56211/buana.v1i1.340.
- [100] Shi H., Xian G., Auch R., Gallo K., Zhou Q.: *Urban heat island and its regional impacts using remotely sensed thermal data a review of recent developments and methodology.* Land, vol. 10(8), 2021, 867. https://doi.org/10.3390/land10080867.
- [101] Darmawan S., Nurulhakim N.N., Hernawati R.: *Kecerdasan Buatan berbasis Geospasial (GeoAI) menggunakan Google Earth Engine untuk Monitoring Fenomena Urban Heat Island di Indonesia* [Geospatial Artificial Intelligence (GeoAI) Using Google Earth Engine for Monitoring the Urban Heat Island Phenomenon in Indonesia]. ELKOMIKA: Jurnal Teknik Energi Elektrik, Teknik Telekomunikasi, & Teknik Elektronika, vol. 12(2), 2024, 303. https://doi.org/10.26760/elkomika.v12i2.303.
- [102] Ramakreshnan L., Aghamohammadi N., Fong C.S., Lee L.H., Ng E., Wong N.H.: *A critical review of urban heat island phenomenon in the context of Greater Kuala Lumpur, Malaysia*. Sustainable Cities and Society, vol. 39, 2018, pp. 99–113. https://doi.org/10.1016/j.scs.2018.02.005.
- [103] Shen Y., Xu Y., Kong W., Li X., Zhang H., Wang J., Chen L.: *Using GeoAI to reveal the contribution of urban park green space features to mitigate the heat island effect*, [in:] Dokonal W., Hirschberg U., Wurzer G. (eds.), *eCAADe 2023: Digital Design Reconsidered, Volume 2, Proceedings of the 41st Conference on Education and Research in Computer Aided Architectural Design in Europe, 20–22 September 2023, Graz University of Technology, Graz, Austria, eCAADe and Graz University of Technology Faculty of Architecture, 2023, pp. 49–58.*
- [104] Mohamed O.Y.A., Zahidi I.: Artificial intelligence for predicting urban heat island effect and optimising land use/land cover for mitigation: Prospects and recent advancements. Urban Climate, vol. 55, 2024, 101976. https://doi.org/10.1016/j.uclim.2024.101976.
- [105] Degefu M.A., Argaw M., Feyisa G.L., Degefa S.: *Regional and urban heat island studies in megacities: A systematic analysis of research methodology.* Indoor and Built Environment, vol. 31(7), 2022, pp. 1775–1786. https://doi.org/10.1177/1420326X211061491.
- [106] Babalola O.S., Akinsanola A.A.: Change detection in land surface temperature and land use land cover over Lagos Metropolis, Nigeria. Journal of Remote Sensing & GIS, vol. 5(3), 2016, 1000171. https://doi.org/10.4172/2469-4134.1000171.
- [107] Kunkel K.E., Changnon S.A., Reinke B.C., Pielke R.A., Changnon D., Sylves R.T., Arritt R.W.: *The July 1995 heat wave in the Midwest: A climatic perspective and critical weather factors*. Bulletin of the American Meteorological Society, vol. 77(7), 1996, pp. 1507–1518. https://doi.org/10.1175/1520-0477 (1996)077<1507:TJHWIT>2.0.CO;2.

- [108] Conti S., Meli P., Minelli G., Solimini R., Toccaceli V., Vichi M., Beltrano C., Perini L.: *Epidemiologic study of mortality during the summer 2003 heat wave in Italy*. Environmental Research, vol. 98(3), 2005, pp. 390–399. https://doi.org/10.1016/j.envres.2004.10.009.
- [109] Wu L., Tajima Y., Yamanaka Y., Shimozono T., Sato S.: *Study on characteristics of SAR imagery around the coast for shoreline detection*. Coastal Engineering Journal, vol. 61(2), 2018, pp. 152–170. https://doi.org/10.1080/21664250.2018. 1560685.